(Received 6 March 2025, Accepted 18 April 2025, Scheduled 5 May 2025)

Design and Performance Analysis of a Miniaturized Four-Port MIMO Antenna Module for 5G NR and WLAN Bands

Jiaping Lu, Lefei He, Qiangjuan Li, and Gui Liu*

College of Electrical and Electronic Engineering, Wenzhou University, Wenzhou 325035, Zhejiang, China

ABSTRACT: This paper presents the design and in-depth performance analysis of a miniaturized four-port multiple-input multiple-output (MIMO) antenna module intended for integration on the rear cover of mobile devices. The four antenna elements are configured in a sequential rotation layout and fabricated on a low-profile circular substrate. Each antenna element features an E-shaped patch on the upper side of the substrate, coupled with a rectangular defected ground structure (DGS) on the lower side. A needle-like decoupling mechanism has been incorporated to improve the isolation between the antenna elements. The measured −10 dB impedance bandwidth ranges from 3.5 to 5.45 GHz, successfully meeting the demands of the 5G NR bands N77 (3.3–4.2 GHz), N78 (3.3–3.8 GHz), N79 (4.4–5 GHz), as well as the wireless local area network (WLAN) band (5.15–5.35 GHz). The isolation levels between the antenna elements exceed 17 dB. The average total efficiency is over 40.76%, and the envelope correlation coefficients (ECCs) are maintained below 0.01. The measurement outcomes indicate that the proposed MIMO antenna not only fulfills the requirements for the 5G and WLAN frequency bands but also successfully achieves miniaturization and superior wireless communication performance.

1. INTRODUCTION

The physical dimensions and shapes of 5G devices are diverse, encompassing but not limited to smart tablets, smartwatches, smart glasses, and smartphones. Given its ability to achieve higher channel capacity within a relatively small footprint, MIMO technology is expected to be extensively utilized in 5G terminal devices. In the field of 5G terminal MIMO antenna design, the primary challenges are to achieve a compact size, multi-band or wideband compatibility, and superior isolation characteristics. Ref. [1] presents the design of an eight-port MIMO antenna on the metal frame of a smartphone, which supports 5G NR bands N77/N78/N79 as well as the WLAN 5 GHz band. However, the proposed MIMO antenna occupies a significant area of the metal frame. Impedance matching and reactance loading techniques have been employed to reduce the antenna dimension and enhance bandwidth [2]. Ref. [3] proposes a compact self-decoupling MIMO antenna. However, it operates in a single frequency band which cannot fulfil the multi-band requirement.

Therefore, designing a compact MIMO antenna array capable of covering several 5G NR bands for mobile devices such as smartphones remains a significant challenge. Such designs must fully utilize the limited space and minimize the impact on device aesthetics and user experience [4, 5]. The performance of an antenna is closely tied to its physical size. To cover a wider range of frequencies, the antenna usually needs to be larger. As the trend towards miniaturization of devices continues and the need to efficiently utilize the internal space of mobile phones grows, the usage of miniaturized and low-profile antennas has become a focal point of research and industry practice [6–11]. Moreover, by exciting multiple resonant points and combining their frequency ranges, the bandwidth of antennas can be effectively enlarged [12, 13]. Enhancing the isolation performance of MIMO antennas is also a current research focus [14]. Techniques such as the use of parasitic elements, decoupling networks, DGS, and self-decoupling technologies significantly improve the isolation of MIMO antenna systems [15–17].

This paper proposes a planar four-antenna module with miniaturization and wideband performance, which can be implemented on the back cover of the mobile terminals. The radiators of four antenna elements are arranged in a circular pattern on the upper surface of a dielectric substrate, with each antenna element positioned 90 degrees apart from the others around the center of the substrate. To attenuate mutual coupling between antenna elements, needle-shaped slots are introduced on the defecated ground plane and improve the impedance matching. The proposed MIMO antenna array has a relatively small area, with a radius of 25 mm and a height of 0.8 mm, smaller than many reported 5G antennas. The measured MIMO antenna frequency band is 3.5–5.45 GHz, working in the required 5G N77, N78, N79 and WLAN (5.15–5.35 GHz) frequency bands. The measured isolation exceeds 17 dB. There is significant coherence between simulated and measured curves.

2. ANTENNA GEOMETRY

Figure 1 illustrates the geometric design of a four-port MIMO antenna array. The presented MIMO antenna array is arranged in a circular FR4 substrate with a radius of 25 mm, a thickness of 0.8 mm, a dielectric constant of 4.4, and a loss tan-

* Corresponding author: Gui Liu (iitgliu2@gmail.com).

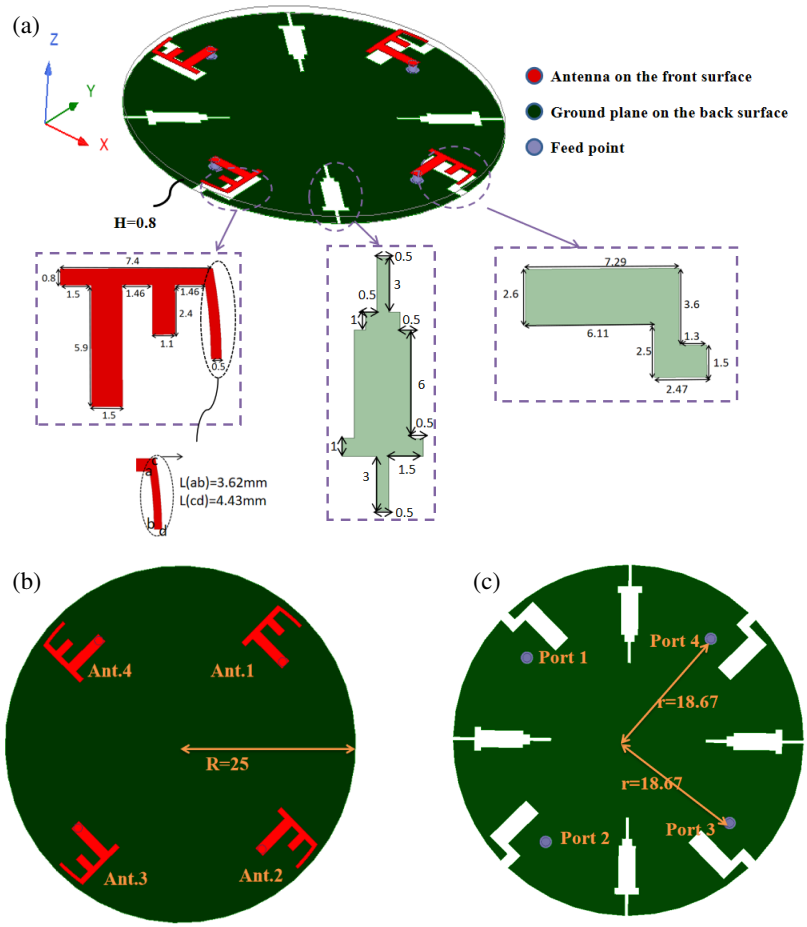

FIGURE 1. Configuration of the proposed antenna. (Unit: mm). (a) The overall structure and geometric dimensions of the proposed MIMO antenna. (b) Top view. (c) Bottom view.

gent of 0.02. As shown in Figure 1(b), each antenna element consists of an E-shaped radiator on the upper surface of the dielectric substrate. The four antenna units are arranged in a sequential 90° rotational manner to achieve physical and phase separation, thereby reducing the coupling between antenna elements. This configuration is capable of exciting multimode resonances, enhancing the broadband properties. The E-shaped radiator is connected to the lower surface through a via, and then connected to the SMA connector. The E-shaped patch can be equivalently represented as a combination of multiple inductors and capacitors. The length of the main trunk (5.9 mm) and the branch sections influence the equivalent inductances. By adjusting these dimensions, the resonant frequency of the E-shaped patch can be changed, as the equivalent inductances and capacitances are altered. Increasing the electrical length through different branches enables resonance at lower frequencies, which helps achieve miniaturization and wideband operation. As depicted in Figure 1(c), each antenna element has a Z-shaped slot which is etched on the lower surface of the substrate. On the metal surface, current usually flows along the shortest path. However, a Z-shaped slot forces the current to flow along its shape, concentrating the current at the slot edges. To further reduce mutual coupling and improve impedance matching, needle-shaped slots are introduced to control the current flow path. The proposed antenna design offers significant isolation and wideband operational capabilities, making it an ideal MIMO antenna solution for 5G communication systems.

3. DESIGN EVOLUTION PROCESS AND ANALYSIS

Figure 2 shows the key design evolution of proposed MIMO antenna. In Case 1, four antenna elements are arranged in a

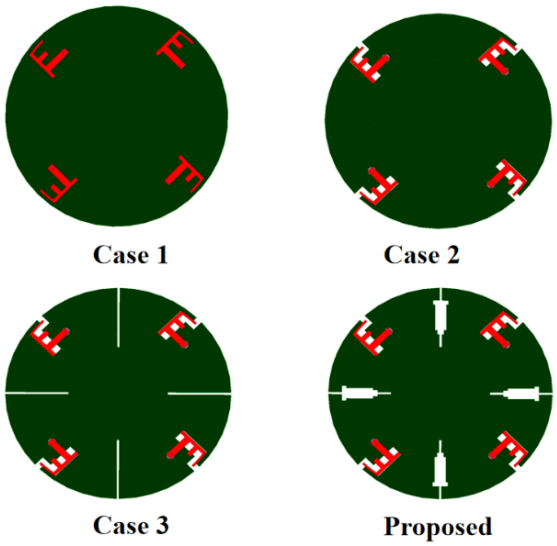

FIGURE 2. Four-port MIMO antenna array design process.

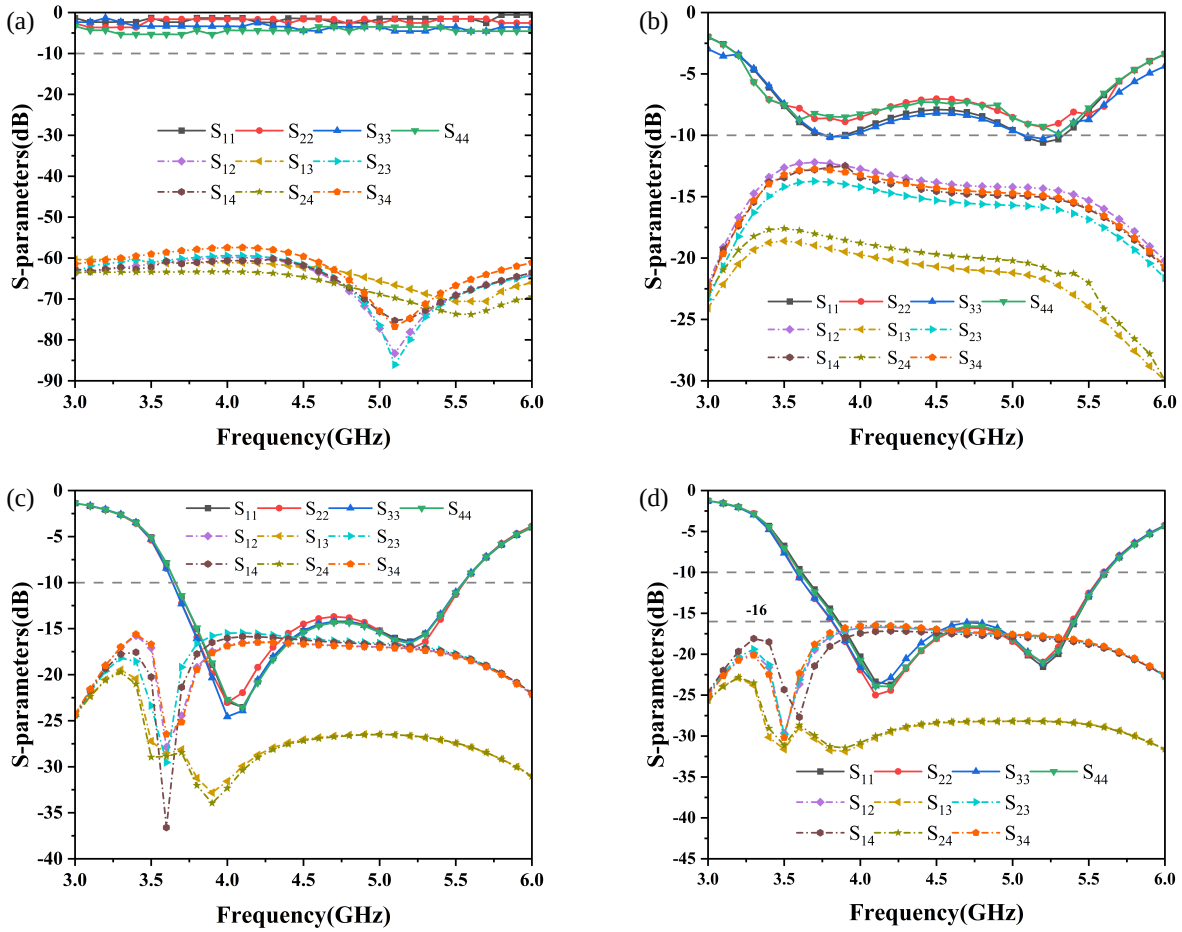

FIGURE 3. The S parameters of the design process are simulated. (a) Case 1. (b) Case 2. (c) Case 3. (d) Proposed.

sequential rotation on the upper surface of the substrate, with a circular metal ground plane on the lower surface. In Case 2, building on Case 1, Z-shaped slots are etched beneath each antenna element. These Z-shaped slots can alter the distribution of surface currents on the ground plane. In Case 3, based on Case 2, four rectangular slots are etched on the ground plane. Finally, based on Case 3, in the proposed MIMO antenna, the four rectangular slots in Case 3 are changed to needle-shaped slots.

Figure 3 shows the simulated S-parameters for every case of the design process, utilizing high-frequency structure simulator (HFSS) as the electromagnetic simulator. In Figure 3(a), it is evident that it fails to meet the requirements for any operational frequency band. In Figure 3(b), the Z-shaped slots introduce two resonances at 4 GHz and 5 GHz for -6 dB impedance bands. As depicted in Figure 3(c), four rectangular slots on the ground plane further improve the -10 dB impedance bandwidth. To further improve the isolation, the needle-shaped slots are employed in the proposed MIMO antenna structure. As shown in Figure 3(d), the S_{11}, S_{22}, S_{33}, and S_{44} curves are nearly identical, indicating excellent consistency and symmetry among them. The proposed MIMO antenna exhibits an operating frequency band range of 3.6–5.6 GHz, successfully meeting the frequency band requirements for 5G NR bands N77 (3.3–4.2 GHz), N78 (3.3–3.8 GHz), N79 (4.4–5.0 GHz), as well as the WLAN band (5.15–5.35 GHz). The isolation between each pair of antenna elements exceeds 16 dB, with particularly impressive isolation for S_{13} and S_{24}, surpassing 25 dB.

In order to further understand the proposed antenna operating principle, the electric field distribution at two resonant frequencies during the design process is depicted in Figure 4. At 4 GHz, the simulated minimum electric field distribution is mainly concentrated in the middle rectangular region of the inverted E-shaped radiating element. At 5 GHz, the lower electric field intensity is distributed at the left corner of the radiating element, while the higher intensity electric fields are dispersed in the lower left and upper right portions of the antenna unit. These high-field-strength regions are where electromagnetic energy concentrates and are potential interference sources. If multiple antennas are close to each other, the strong electric fields in these regions can easily couple to adjacent antennas, reducing the isolation. By using the electric-field distribution diagram to locate these problem areas, a basis for improvement can be provided. Eventually, the electric field distribution among antennas becomes more discrete, and the mutual interference of the electric fields near each antenna is reduced, thus improving the corresponding isolation. Therefore, optimizing the geometric parameters affecting the performance of the MIMO antenna can be based on the electric field distribution.

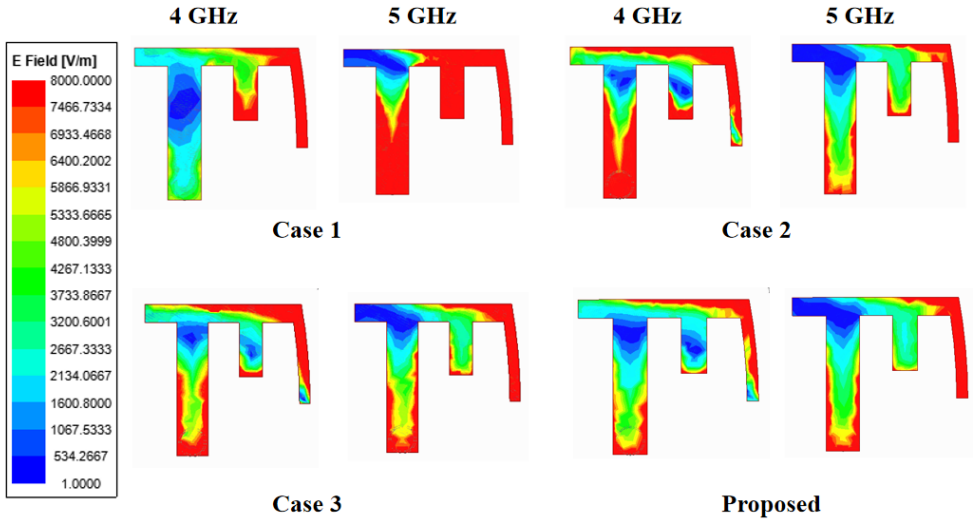

FIGURE 4. Simulated E-field distribution at two resonant frequencies.

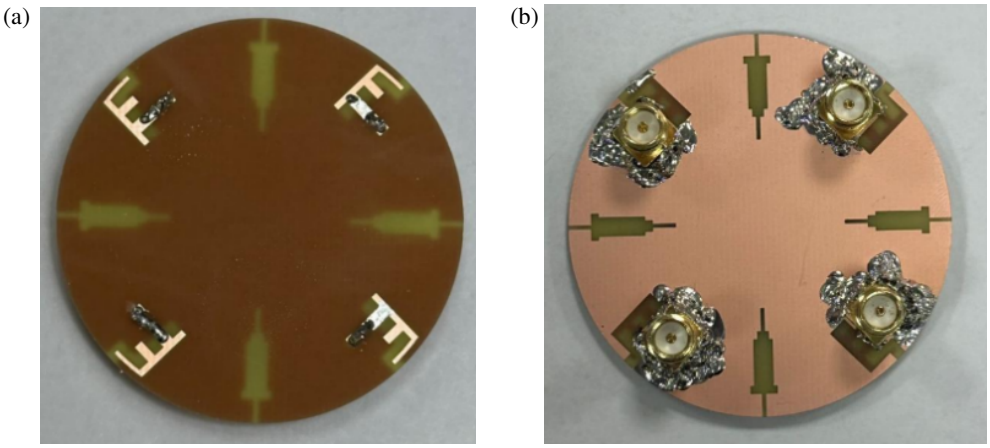

FIGURE 5. Photographs of the fabricated antenna. (a) Top view. (b) Bottom view.

4. EXPERIMENTAL RESULTS AND DISCUSSION

Figure 5 shows photographs of the fabricated four-port MIMO antenna prototype. The S-parameters were measured by a Keysight vector network analyzer (VNA: N5223A), and the 2D radiation patterns were measured in an anechoic chamber. The measured reflection and transmission coefficients of the fabricated MIMO antenna are shown in Figure 6. Compared to the simulation results in Figure 3(d), noticeable deviations between the measured and simulated results are observed, which is due to manufacturing tolerances and inherent losses of the substrate. The measurements show that the -10 dB impedance bandwidth is 1.95 GHz, ranging from 3.5 GHz to 5.45 GHz. The measured isolation within the operating band is larger than 17 dB. Therefore, the antenna prototype demonstrates good performance within the desired frequency range, fulfilling the requirements for low reflection loss and high isolation.

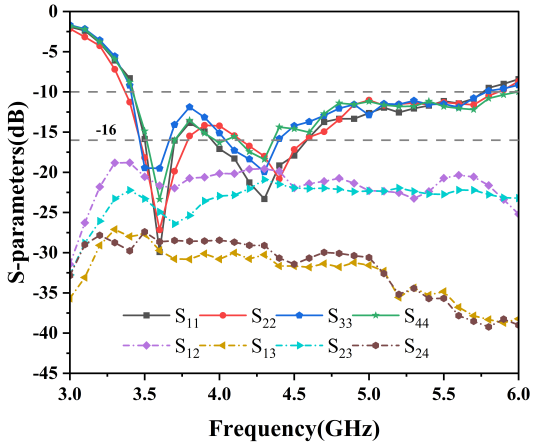

FIGURE 6. Measured S-parameters of the fabrication antenna.

To further validate the performance of the fabricated MIMO antenna, Figure 7 illustrates the normalized radiation patterns in the E-plane and H-plane at frequencies of 4 GHz and 5 GHz. The solid lines represent simulated results, while the dashed lines correspond to the measured data. The red curves signify cross-polarization (X-pol), and the blue curves indicate co-polarization (Co-pol). The discrepancies between the sim-

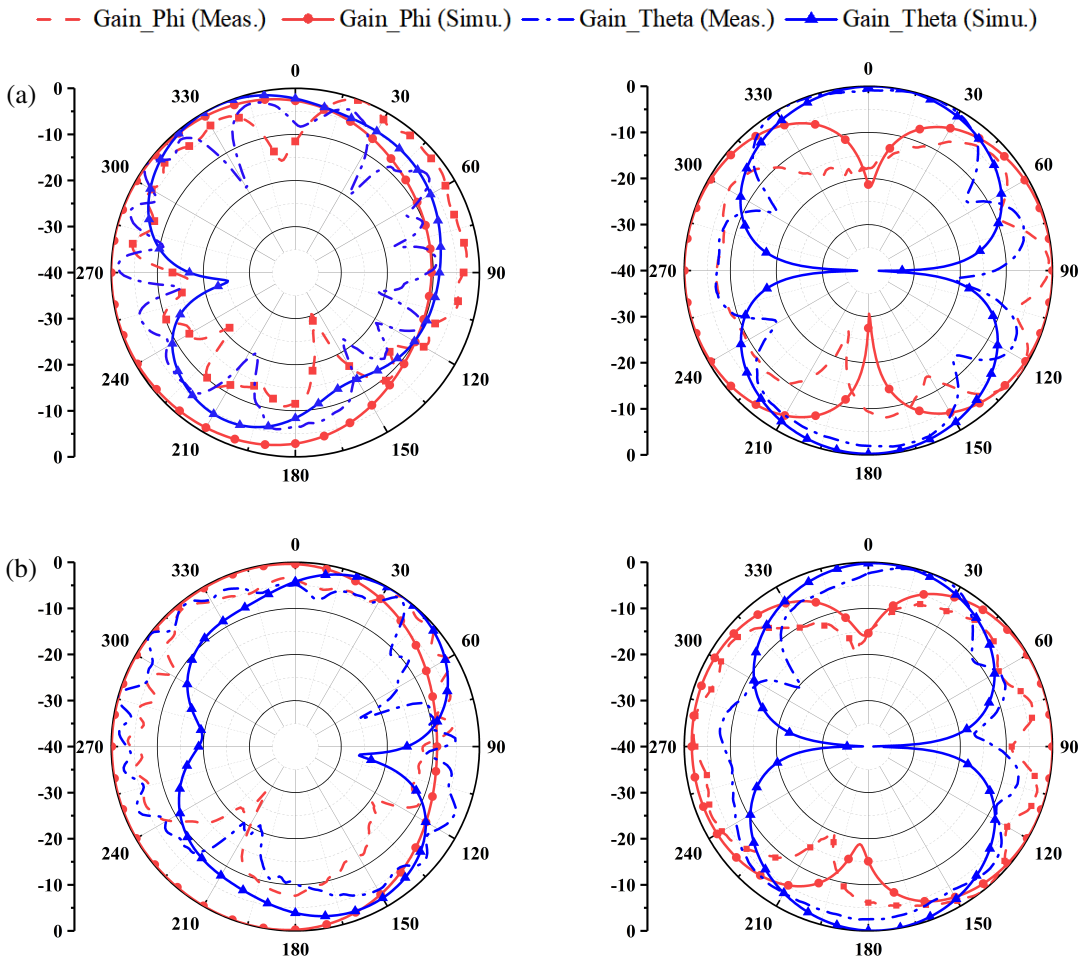

FIGURE 7. Measured and simulated normalized two-dimensional radiation patterns in the E-plane and H-plane at (a) 4 GHz, (b) 5 GHz.

ulation and measurement curves in Figure 7 can be primarily attributed to variations in the welding process and inconsistencies in the mounting angles encountered during antenna testing within the anechoic chamber. The co-polarized component of the antenna typically reflects the primary radiation direction, while the cross-polarized component serves as an indicator for assessing background noise and unintended radiation. The two-dimensional patterns reveal that the MIMO design exhibits nearly omnidirectional radiation in the E-plane and bidirectional radiation in the H-plane.

Envelope Correlation Coefficient (ECC) is a crucial metric for assessing the performance of MIMO antennas. It quantifies the correlation between two radiation elements. A lower ECC value indicates that the antenna possesses favorable MIMO correlation and superior diversity performance. As depicted in Figure 8(a), the ECC values within 3.5–5.45 GHz frequency band are less than 0.01. This is well below the threshold of 0.5, which is the standard criterion for the normal operation of MIMO antennas. The ECC value is computed using Equation (1).

$$\rho_c(i,j) = \frac{\left| \iint\limits_{4\pi} \left[F_i(\theta,\varphi) \cdot F_j^*(\theta,\varphi) \right] d\Omega \right|^2}{\iint\limits_{4\pi} \left| F_i(\theta,\varphi) \right|^2 d\Omega \cdot \iint\limits_{4\pi} \left| F_j(\theta,\varphi) \right|^2 d\Omega} \quad (1)$$

Diversity gain (DG) can be calculated using Equation (2), and it is directly affected by the ECC value. Figure 8(b) illustrates the calculated DG of the proposed MIMO antenna. It is evident that the DG value surpasses 9.99 dB throughout the frequency band of interest.

$$DG = 10 \times \sqrt{1 - |ECC|^2} \quad (2)$$

Channel capacity loss (CCL) is a key diversity parameter that affects the upper limit of achievable communication transmission rates. To evaluate the CCL of the proposed MIMO antenna, it can be calculated using Equations (3)–(6). Figure 8(c) shows the CCL of the proposed MIMO antenna. It is evident that the CCL value remains below 0.3 across the frequency band of interest, indicating that the proposed MIMO antenna achieves a highly favorable channel transmission rate.

$$C_{loss} = -\log_2[\det(\psi^R)] \quad (3)$$

$$\psi^R = \begin{bmatrix} \rho_{ii} & \rho_{ij} \\ \rho_{ji} & \rho_{jj} \end{bmatrix} \quad (4)$$

$$\rho_{ii} = (1 - |S_{ii}|^2 - |S_{ij}|^2 \quad (5)$$

$$\rho_{ij} = -(S_{ii}^* S_{ij} + S_{ji}^* S_{ij}) \quad \text{for } i,j = 1 \quad \text{or } 2 \quad (6)$$

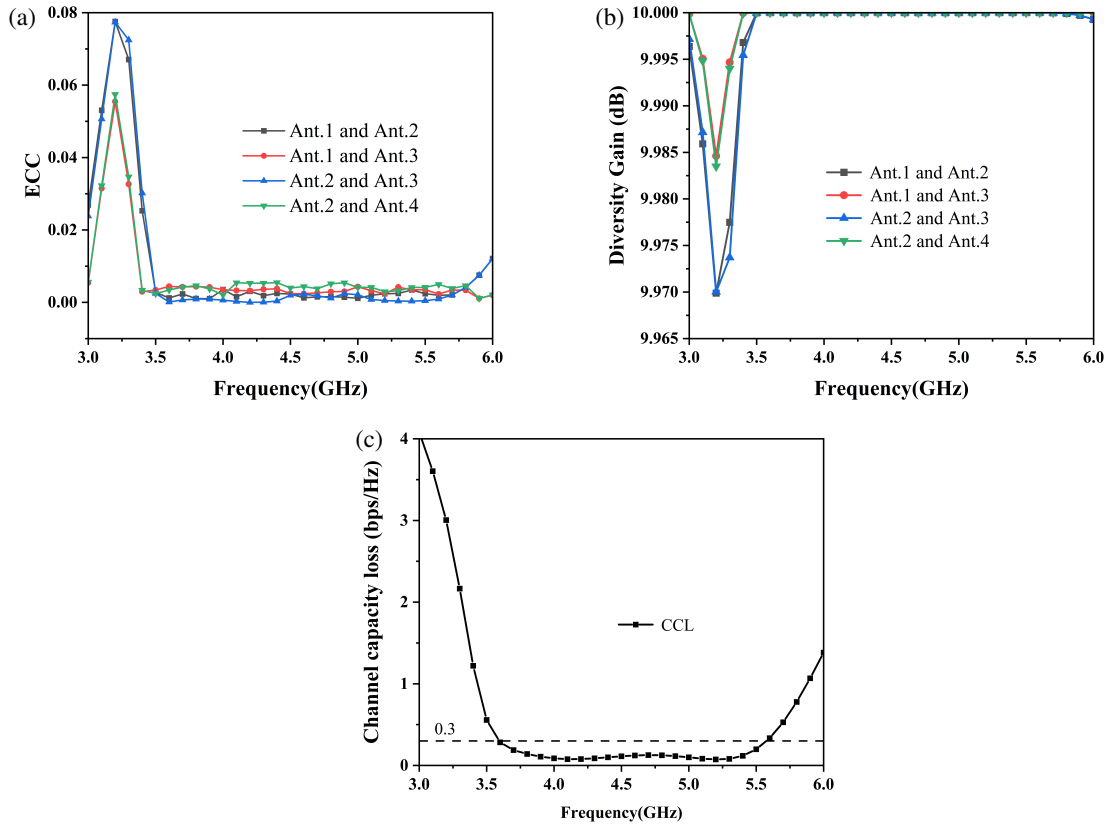

FIGURE 8. MIMO parameters. (a) ECC. (b) DG. (c) CCL.

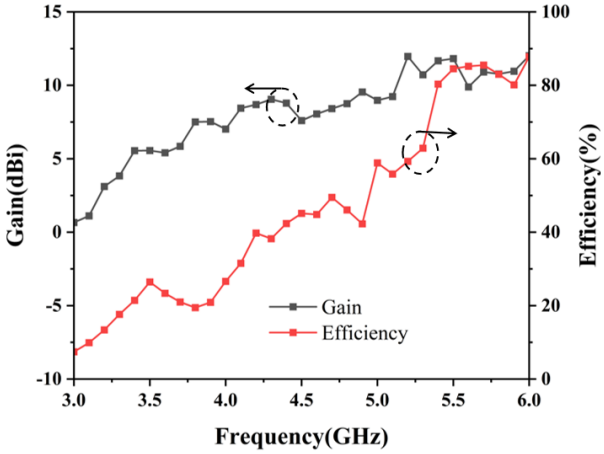

FIGURE 9. The measured gain and efficiency of this antenna.

Figure 9 presents the measured gain and efficiency. The gain exceeds 5.41 dBi, while the total efficiency increases over the desired frequency range, with a maximum exceeding 85%.

In Table 1, the performance of the proposed MIMO antenna is compared with other published miniaturized 5G MIMO antennas in [7–9, 18–20]. The primary contribution of our work is the introduction of a MIMO antenna solution that features a larger bandwidth and higher isolation, along with a lower profile, while maintaining comparable MIMO antenna performance.

TABLE 1. Comparison of the proposed design with some referenced works.

Reference	Operating band (GHz)	Isolation (dB)	Height (mm)	Port number	Area (mm^2)
[7]	3.3–4.2	> 10	2.4	4	1600
[8]	3.3–4.2	> 9.7	2	4	753.4
[9]	3.3–4.2	> 14	10	3	2500
[18]	3.3–4.2	> 9.5	1	4	1764
[19]	3.3–4.2	> 15	10	3	/
[20]	3.3–5 (-6 dB)	> 10	2	4	1764
Proposed	3.5–5.45	> 17	0.8	4	1963.5

5. CONCLUSION

In order to alleviate the limitations on the bezels of 5G mobile terminals, this paper proposes a miniaturized, high-isolation, and wideband four-port MIMO antenna that can be integrated on the back cover of mobile devices. The four antenna elements are configured in a sequential rotation pattern, forming the proposed MIMO antenna. The antenna module is designed with a circular shape and a low profile, making it an ideal solution for space-constrained device designs. The measured -10 dB impedance bandwidth is 1.95 GHz, ranging from 3.5 GHz to 5.45 GHz. It successfully covers the 5G N77/N78/N79 bands and WLAN 5-GHz band. Moreover, the isolation between antenna elements is over 17 dB, and the diversity gain (DG) value exceeds 9.99 dB. The envelope correlation coefficient (ECC)

and mean cross-correlation coefficient (CCL) values within the 3.5–5.45 GHz frequency band are less than 0.01 and 0.3, respectively. The consistency between the simulated and measured curves is remarkable, which verifies the effectiveness of the proposed antenna design. This design provides a reliable and efficient approach to enhance wireless communication capabilities in compact device configurations, offering significant potential for the development of next-generation mobile communication devices.

ACKNOWLEDGEMENT

This work was supported in part by the National Natural Science Foundation of China under Grant No. 6167133, the Science and Technology Department of Zhejiang Province under Grant No. LGG19F010009, and Wenzhou Municipal Science and Technology Program under Grant No. 2018ZG019.

REFERENCES

[1] Chen, H.-D., Y.-C. Tsai, C.-Y.-D. Sim, and C. Kuo, "Broadband eight-antenna array design for sub-6 GHz 5G NR bands metal-frame smartphone applications," *IEEE Antennas and Wireless Propagation Letters*, Vol. 19, No. 7, 1078–1082, 2020.

[2] Cai, Q., Y. Li, X. Zhang, and W. Shen, "Wideband MIMO antenna array covering 3.3–7.1 GHz for 5G metal-rimmed smartphone applications," *IEEE Access*, Vol. 7, 142 070–142 084, 2019.

[3] Ren, Z., A. Zhao, and S. Wu, "MIMO antenna with compact decoupled antenna pairs for 5G mobile terminals," *IEEE Antennas and Wireless Propagation Letters*, Vol. 18, No. 7, 1367–1371, 2019.

[4] Li, Y., C.-Y.-D. Sim, Y. Luo, and G. Yang, "High-isolation 3.5 GHz eight-antenna MIMO array using balanced open-slot antenna element for 5G smartphones," *IEEE Transactions on Antennas and Propagation*, Vol. 67, No. 6, 3820–3830, 2019.

[5] Zhang, X., Y. Li, W. Wang, and W. Shen, "Ultra-wideband 8-port MIMO antenna array for 5G metal-frame smartphones," *IEEE Access*, Vol. 7, 72 273–72 282, 2019.

[6] Wong, K.-L., J.-Z. Chen, and W.-Y. Li, "Four-port wideband annular-ring patch antenna generating four decoupled waves for 5G multi-input-multi-output access points," *IEEE Transactions on Antennas and Propagation*, Vol. 69, No. 5, 2946–2951, 2021.

[7] Wong, K.-L., M.-F. Jian, and W.-Y. Li, "Low-profile wideband four-corner-fed square patch antenna for 5G MIMO mobile antenna application," *IEEE Antennas and Wireless Propagation Letters*, Vol. 20, No. 12, 2554–2558, 2021.

[8] Chang, L. and H. Wang, "Miniaturized wideband four-antenna module based on dual-mode PIFA for 5G 4 × 4 MIMO applications," *IEEE Transactions on Antennas and Propagation*, Vol. 69, No. 9, 5297–5304, 2021.

[9] Wong, K.-L., C.-M. Chou, Y.-J. Yang, and K.-Y. Wang, "Multipolarized wideband circular patch antenna for fifth-generation multi-input-multi-output access-point application," *IEEE Antennas and Wireless Propagation Letters*, Vol. 18, No. 10, 2184–2188, 2019.

[10] Sasikumar, J. and V. Koushick, "Performance analysis of complementary split ring resonator with improved four element antenna for X band wireless applications," *Progress In Electromagnetics Research M*, Vol. 130, 95–102, 2024.

[11] Ali, A., M. Rasool, M. Z. Zahid, I. Rashid, A. M. Siddique, M. Maqsood, and F. A. Bhatti, "A 4-port broadband high-isolated MIMO antenna for wireless communication," *Progress In Electromagnetics Research C*, Vol. 142, 119–130, 2024.

[12] Cheng, B., Z. Du, and D. Huang, "A broadband low-profile multimode microstrip antenna," *IEEE Antennas and Wireless Propagation Letters*, Vol. 18, No. 7, 1332–1336, 2019.

[13] Liang, C.-F., Y.-P. Lyu, D. Chen, W. Zhang, and C.-H. Cheng, "A low-profile and wideband circularly polarized patch antenna based on TM11 and TM21," *IEEE Transactions on Antennas and Propagation*, Vol. 69, No. 8, 4439–4446, Aug. 2021.

[14] Liu, G., C. Zhang, Z. Chen, and B. Chen, "A compact dual band MIMO antenna for 5G/WLAN applications," *International Journal of Microwave and Wireless Technologies*, Vol. 14, No. 10, 1347–1352, 2022.

[15] Zhao, A. and Z. Ren, "Size reduction of self-isolated MIMO antenna system for 5G mobile phone applications," *IEEE Antennas and Wireless Propagation Letters*, Vol. 18, No. 1, 152–156, 2019.

[16] Huang, J., T. He, S. Xi, Q. Yang, X. Shi, and G. Liu, "Eight-port high-isolation antenna array for 3.3–6 GHz handset applications," *AEU — International Journal of Electronics and Communications*, Vol. 154, 154333, 2022.

[17] Zhang, C., J. Huang, X. Shi, G. Dong, J. Cai, and G. Liu, "A compact ultra-thin 4 × 4 multiple-input multiple-output antenna," *Sensors*, Vol. 22, No. 16, 6091, 2022.

[18] Barani, I. R. R., K.-L. Wong, Y.-X. Zhang, and W.-Y. Li, "Low-profile wideband conjoined open-slot antennas fed by grounded coplanar waveguides for 4 × 4 5G MIMO operation," *IEEE Transactions on Antennas and Propagation*, Vol. 68, No. 4, 2646–2657, Apr. 2020.

[19] Wong, K.-L., H.-J. Chang, J.-Z. Chen, and K.-Y. Wang, "Three wideband monopolar patch antennas in a Y-shape structure for 5G multi-input–multi-output access points," *IEEE Antennas and Wireless Propagation Letters*, Vol. 19, No. 3, 393–397, Mar. 2020.

[20] Cheng, S.-H., S.-C. Chen, and W.-Y. Huang, "Low-profile MIMO trapezoidal patch antenna for 5G wideband mobile antenna application," *IEEE Antennas and Wireless Propagation Letters*, Vol. 24, No. 3, 696–700, Mar. 2025.